Applied Catalysis B: Environmental 150–151 (2014) 380–388

Contents lists available at ScienceDirect

Applied Catalysis B: Environmental

journal homepage: www.elsevier.com/locate/apcatb

Bismuth oxybromide promoted detoxification of cylindrospermopsin under UV and visible light illumination

Shulian Wang[a,b], Wanhong Ma[a], Yanfen Fang[a], Manke Jia[a], Yingping Huang[a,*]

[a] Engineering Research Center of Eco-environment in Three Gorges Reservoir Region, Ministry of Education, China Three Gorges University, Yichang 443002, China

[b] Institute of Hydrobiology, Chinese Academy of Sciences, Wuhan 430072, China

ARTICLE INFO

Article history:
Received 17 September 2013
Received in revised form
23 November 2013
Accepted 8 December 2013
Available online 21 December 2013

Keywords:
Cylindrospermopsin
Uracil
BiOBr
Degradation
Mechanism

ABSTRACT

Bismuth oxybromide (BiOBr) was prepared and characterized by X-ray diffraction (XRD), scanning electron microscope (SEM), X-ray photoelectron spectroscopy (XPS) and UV–vis diffuse reflectance spectroscopy (DRS). The BiOBr promoted detoxification of cylindrospermopsin (CYN) under UV ($\lambda < 350$ nm) and visible light ($\lambda > 420$ nm) illumination was studied. The results revealed that the toxic uracil unit of CYN was removed, and the carboxylic group of the degraded product was also decomposed, to give the innoxious tricyclic guanidine product under the title conditions. In contrast, the traditional Fenton reagents (Fe^{2+} and H_2O_2) limited to remove the uracil moiety of CYN with the carboxylic group intact. Presumably, the decarboxylation ability of BiOBr was induced by Br 4*p* valence band hole ($h_{Br\,4p}^{+}$), and the degradation mechanism was also proposed based on the experimental results and theoretical calculation.

1. Introduction

The potential hazard of cyanobacterial toxins is demonstrated by livestock poisoning and human death due to drink the water containing high concentration of cyanobacteria [1]. Cyanobacteria, also known as blue-green algae, are prokaryotic organisms growing in freshwaters and brackish lakes. The toxic cyanotoxins are the secondary metabolites of cyanobacteria [2]. Cylindrospermopsin (CYN) is one of the common members of cyanotoxins which always cause human injury. CYN originates from several cyanobacteria, such as *Cylindrospermopsis raciborskii* [3], *Umezakia natans* [4], *Aphanizomenon ovalisporum* [5], *Anabaena bergii* [6], *Raphidiopsis curvata* [7], *Aphanizomenon flos-aquae* [8], *Anabaena lapponica* [9], *Lyngbya wollei* [10] and *Aphanizomenon gracile* [11]. CYN has neurotoxic effects (inhibition of protein synthesis by binding to liver DNA and forms single DNA adducts which results in liver damage), hepatotoxic effects (inhibition of glutathione synthesis in hepatocytes), and cytotoxic effects (inhibitor of cytochrome P450) [12]. CYN belongs to guanidine alkaloids, and the molecular structure contains tricyclic guanidine moiety and hydroxymethyl uracil (see Fig. 1). CYN acts to inhibit various enzymatic reactions by competing for the binding site of uridine diphosphate (UDP), which serves as a glycosyl group carrier in higher animals. The uracil moiety of CYN structurally resembles the uridine moiety of UDP [13]. The toxicity of CYN comes from the uracil unit, so the decomposition of uracil is regarded as the general method to detoxify it.

As global warming, CYN spreads from the tropics to temperate zone, the peak concentration of CYN can be found in the aqueous media toward the end of a water bloom when the algae are still viable [14]. This phenomena and hazard cause scientific attention on the detoxification of it. The traditional water treatment processes, such as coagulation, flocculation and filtration are ineffective to remove the toxic CYN [15,16]. Some cyanobacterial toxins can be removed by activated carbon via physical adsorption, however, the limited adsorption ability and high cost of activate carbon inhibit its practical application [17]. The effective chemical degradation of CYN by chlorination [18–21] and ozonation [22] has also been realized, but suffering from long degradation time and high cost. Recently, advanced oxidation processes (AOPs) based on high active hydroxyl radical (•OH) have been established as an alternative and superior to conventional chemical oxidation for the degradation of CYN [23]. Among AOPs, photocatalytic degradation with TiO_2 under UV irradiation is an attractive alternative for the detoxification of cyanotoxins [24,25]. However, the wide band gap (3.2 eV for anatase) of TiO_2 results in the absorption within the UV light region. In addition, only a fraction of pollutants are mineralized to CO_2 during the initial phase of TiO_2 photocatalysis, and most of them remain with the toxic groups intact.

In recent years, BiOBr has received remarkable interest in the potential photocatalysis to remove contaminants from aqueous

* Corresponding author. Tel.: +86 717 6397488; fax: +86 717 6395966.
E-mail addresses: huangyp@ctgu.edu.cn, yingpinghuang@126.com (Y. Huang).

0926-3373/$ – see front matter © 2013 Elsevier B.V. All rights reserved.
http://dx.doi.org/10.1016/j.apcatb.2013.12.016

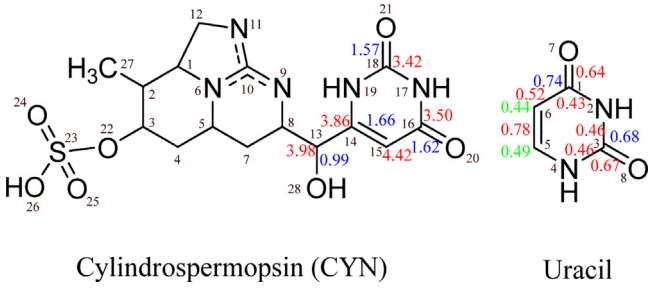

Fig. 1. The structures of CYN and uracil. The red, blue and green numbers represent electron population, bond order and free valence, respectively.

solution, owing to its stability, suitable band gap and relatively superior photocatalytic abilities [26–28]. Both O 2*p* and Br 4*p* states of BiOBr dominate the valence band, whereas Bi 6*p* state contributes the most to the conduction band [29]. Very recently, our group discovered that BiOBr photocatalyst had ability to selectively remove the free carboxylic groups from D-Glu and D-MeAsp of microsystin-LR (MC-LR). In contrast, the TiO_2 photocatalyst cannot do so [30]. BiOBr crystallizes in the tetragonal matlockite structure and has layered structure characterized by $[Bi_2O_2]$ slabs interleaved by double slabs of bromine atoms [31]. Our previous research indicated that BiOBr had two separate valence bands, instead of hybridized valence band, which had different oxidation abilities and responded to UV and visible light, respectively [32]. Furthermore, the valence hole energy of BiOBr (~2.25 V) is not high enough to oxidize H_2O ($E^0_{\bullet OH/H_2O} = +2.7$ V, NHE) [29]. Thus, separate valence bands and lower redox potential could lead to different degradation pathways compared with other AOP systems. Song et al. originally reported the detailed mechanism of degradation and transformation of CYN by •OH generated from γ radiolysis [33]. They found that CYN was detoxified through removal of the uracil moiety. In this paper, we reported BiOBr promoted photocatalytic detoxification of CYN respectively under UV and visible light illumination through decomposition of the uracil unit and decarboxylation from CYN to eliminate its toxicity. As a compare, traditional Fenton system was employed to degrade CYN. The degradation of uracil was also studied as a control experiment to further verify the detoxification mechanism.

2. Materials and methods

2.1. Reagents

CYN and uracil (Fig. 1) were purchased from Express Technology Co. and Aladdin Industrial Inc., respectively. CPB (hexadecylpyridinium bromide) was purchased from Aladdin Industrial Inc. DMPO (5,5-dimethyl-1-pyrroline-*N*-oxide) was obtained from Sigma–Aldrich Co. TiO_2 (Degussa P25), containing 80% anatase and 20% rutile, was used. Chromatographically pure methanol was received from J.T. Baker Co. All reagents were used without further purification. Deionized and redistilled water was used.

2.2. Theoretical calculation of substrate molecules

Semi-empirical method is used to calculate molecular parameters and helpful to seek rules of structure and property. Semi-empirical self-consistent-field molecular orbital method (AM1) and Huckel molecular orbital method (HMO) are widely applied among them [34–36]. Electron population, bond order and free valence are frequently used parameters to evaluate π charge density in organic conjugated systems. Generally, atoms with the highest electron population are the sites easily attacked by electrophilic groups; atoms with the lowest electron population are the sites easily attacked by nucleophilic groups; reactions involved free radicals easily occur at atoms with the highest free valence; nucleophilic, electrophilic and free radical reactions are inclined to occur at atoms with the highest free valence when electron populations are equal. Bond order represents the intensity of bond energy. The higher the bond energy, the more stable the molecules.

AM1 was employed to optimize the geometric configuration and calculate electron population and bond order of CYN. Uracil has planar configuration, so the π electronic structure of it was processed according to HMO. The electron population, bond order and free valence of different atoms were calculated using self-compiled computer program. The numbers of atoms in CYN and uracil were shown in Fig. 1.

2.3. Synthesis and characterization of BiOBr

BiOBr was prepared according to Ref. [30]. In a typical operation, $Bi(NO_3)_3{\cdot}5H_2O$ was dissolved in 1.2 mol/L HNO_3 solution, and 0.05 mol/L CPB aqueous solution was kept in 40 °C temperature bath all the time. The molar ratio of CPB/$Bi(NO_3)_3{\cdot}5H_2O$ was set as 3:2. Yellow precipitates produced when acidic solution of $Bi(NO_3)_3{\cdot}5H_2O$ was added dropwise into the CPB solution. The pH of the mixture was then adjusted to 7 with NaOH (0.5 mol/L) and the solution was vigorously stirred for 1 h at room temperature. Finally, the above solution was heated at 170 °C for 17 h. The resulting precipitates were washed with plenty of water and dried at 50 °C in air.

The crystalline phases of the samples were characterized by Ultima IV XRD (Rigaku, Japan) with Cu K_α radiation (λ = 1.54178 Å). The surface morphology of BiOBr was observed by JSM-7500F field SEM (JEOL, Japan). Surface element compositions were analyzed by an Axis-Ultra DLD multi-technique XPS (Kratos, Britain) employing a monochromated K_α X-ray source ($h\nu$ = 1486.6 eV). The specific surface area was determined by an ASAP 2020 model BET surface area and pore size analyzer (Micrometritics, USA). The DRS of BiOBr was recorded on a U-3010 UV-Vis spectrophotometer (Hitachi, Japan) using spectral grade $BaSO_4$ as the reference material.

2.4. Degradation of CYN and uracil

A 100 W mercury lamp (2.8 mW/m^2) and 500 W halogen lamp (22.9 mW/m^2), purchased from Nanjing Xujiang Electromechanical Plant, were used as the UV light and visible light source, respectively. They were positioned inside the XPA photochemical reaction instrument (Xujiang Electromechanical Plant, China). To ensure that the system was irradiated only by UV light with wavelength below 350 nm, 6 pieces of cutoff filter (17.5 cm × 4.5 cm × 0.2 cm) were placed outside the Pyrex jacket to eliminate any radiation with wavelength above 350 nm. The wavelength of visible light source is above 420 nm.

All the CYN and uracil photocatalytic degradation experiments were carried out in a Pyrex vessel (10 mL) with 5 mL 2 mg/L CYN (uracil) and certain amount of BiOBr. Prior to the irradiation, the suspensions were magnetically stirred in dark for approximately 1 h to ensure that CYN (uracil) reached an adsorption–desorption equilibrium on the surface of BiOBr. At specific time intervals, aliquots (300 μL) were collected, centrifuged, and then filtered through a Millipore filter (pore size 0.22 μm) to remove the solid catalyst particles prior to high performance liquid chromatography (HPLC) analysis.

2.5. Analysis methods

HPLC analysis was performed with a Waters 2998 photodiode array (PDA) detector and a C_{18} reverse-phase column (5 μm; 4.6 mm i.d. × 250 mm, kromasil). Gradient elution for the

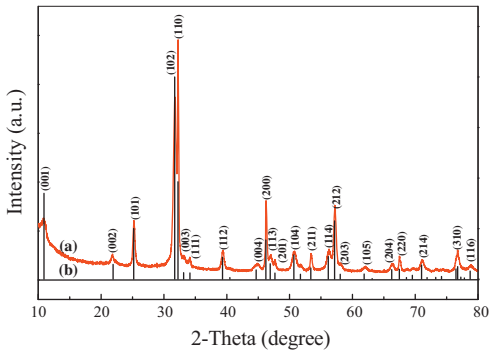

Fig. 2. The XRD patterns of (a) BiOBr as-prepared and (b) standard card (JCPDS card no. 78-0348).

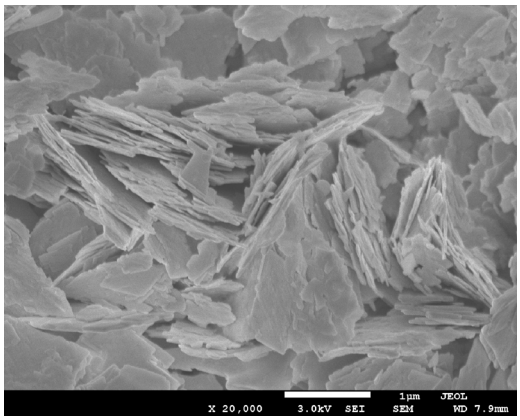

Fig. 3. The SEM image of as-prepared BiOBr.

determination of CYN was started from 2% methanol and 98% water, followed by a linear increase of methanol to reach 20% at 10 min. The injection volume was 20 μL. The flow rate was 0.40 mL/min and the detection wavelength was 262 nm. A liquid chromatography tandem mass spectrometry (LC–MS) instrument (Agilent, USA) with an electrospray ionization (ESI) interface was used to monitor the reaction intermediates by full-scan from m/z 50 to 600 in the positive ion mode.

The degradation of uracil was followed by HPLC with the same column, disodium hydrogen phosphate solution (0.05 mol/L, pH 4.0) and methanol (v:v = 95:5) as mobile phase. The flow rate was 0.80 mL/min and the detection wavelength was 260 nm. LC–MS analysis of uracil was performed by full-scan from m/z 50 to 250 in the positive ion mode.

A Bruker model EPR 300E spectrometer (Bruker, Germany) equipped with a Quanta-Ray Nd:YAG laser (355 and 532 nm) was used for the measurement of the ESR signals of •OH and superoxide radical ($•O_2^-$) spin-trapped by DMPO. Measurement conditions were as follows: center field 3486.7 G, sweep width 100 G, microwave frequency 9.82 GHz, and power 5.05 mW. To minimize experimental errors, the same quartz capillary tube was used for all ESR measurements.

3. Results and discussion

3.1. Characterization of BiOBr

The crystallographic structure of BiOBr was characterized by powder XRD patterns (Fig. 2). All the diffraction peaks in the patterns can be assigned to the tetragonal phase of BiOBr (JCPDS card no.78-0348), displaying a high purity of the product. After refinement, the crystal lattice parameters of BiOBr were calculated to be $a = b = 3.9201$ Å and $c = 8.0984$ Å. The intense and narrow diffraction peaks imply the good crystallinity of the BiOBr samples. The

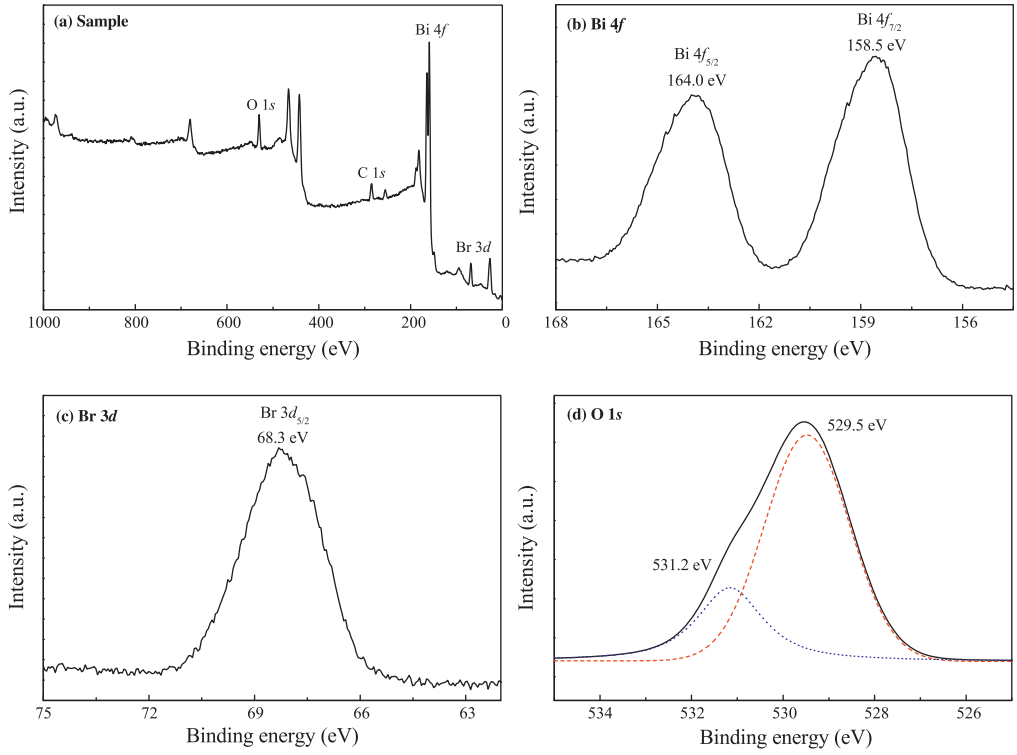

Fig. 4. (a) Full spectrometric surveying, (b) Bi 4*f*, (c) Br 3*d* and (d) O 1*s* XPS spectra of BiOBr.

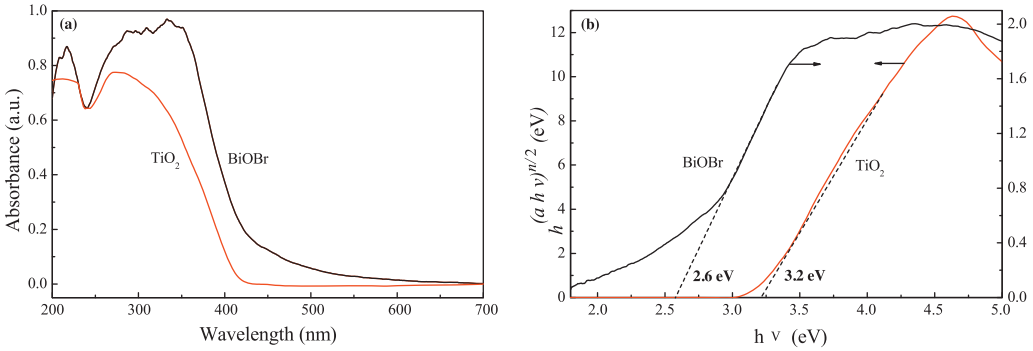

Fig. 5. The (a) DRS and (b) plots of $(\alpha h\nu)^{n/2}$ versus photon energy ($h\nu$) for BiOBr and TiO_2. The values of n for BiOBr and TiO_2 are 4 and 1, respectively.

average crystalline size of BiOBr was calculated to be 28.3 nm according to the Scherrer formula (1) [37]:

$$D = \frac{K\lambda}{\beta \cos\theta} \quad (1)$$

where D is taken as crystalline size (nm), K is Scherrer constant equal to 0.89, β is the half-peak width for BiOBr in radians on the 2θ scale, θ is Bragg angle for the diffraction peaks, λ is the X-ray wavelength (nm).

As shown in Fig. 3, the morphology of BiOBr was characterized by SEM, which indicates that BiOBr has lamellar structure of size 400–500 nm. In addition, the nitrogen adsorption–desorption measurement results show that the BET surface area, pore volume and pore diameter are 12.1 m^2/g, 0.13 cm^3/g and 42.2 nm, respectively.

The element compositions of BiOBr were investigated by XPS analysis. As shown in Fig. 4a, BiOBr is composed of four elements (Bi, O, Br and C). The C peak can be attributed to the adventitious carbon on the surface of BiOBr from disposition. In the high resolution spectrum of Fig. 4b, two strong peaks centered at 164.0 eV and 158.5 eV can be attributed to the binding energy of Bi $4f_{5/2}$ and Bi $4f_{7/2}$, respectively, demonstrating that the main chemical states of Bi element in BiOBr are trivalent. As for the high resolution XPS spectrum of Br 3*d* (Fig. 4c), 68.3 eV is consistent with the binding energy of Br $3d_{5/2}$. O 1*s* curve visibly displays the asymmetrical shape among XPS spectra of three composition elements. After fitting curve of O 1*s*, we obtain two peaks at 531.2 eV and 529.5 eV (Fig. 4d), which are related to the O of Bi_2O_2 unit in BiOBr and other components (such as —OH and H_2O) adsorbed on the surface of BiOBr, respectively [38]. For the latter, the peak area is larger than that of the former, which indicates the excessive loaded —OH or H_2O on the surface of BiOBr.

The DRS of BiOBr is shown in Fig. 5a. It is observed that BiOBr can absorb visible light compared with TiO_2. BiOBr exhibits significant increase in the photo absorption at wavelengths lower than about 470 nm due to the band gap transition, implying the possibility of photocatalytic activity of BiOBr under visible light irradiation. As a crystalline semiconductor, it is well known that the optical

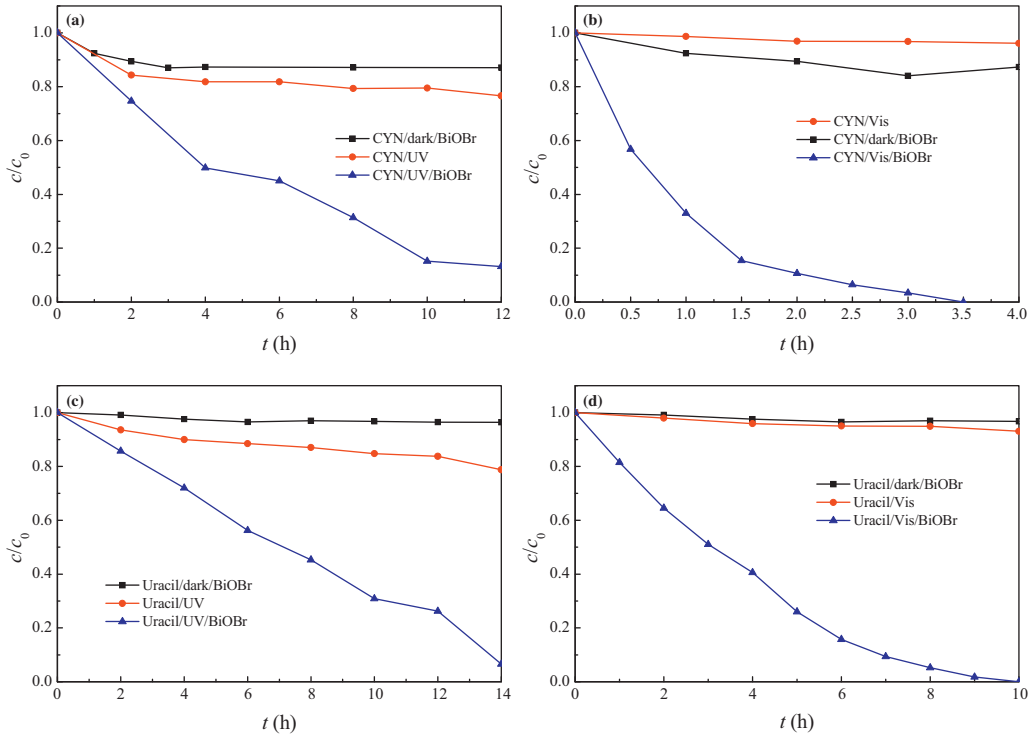

Fig. 6. The degradation of CYN (a and b) and uracil (c and d). Figures (a) and (c) were under UV and figures (b) and (d) were under visible light irradiation. [CYN] = [uracil] = 2 mg/L; [BiOBr] = 0.2 g/L.

absorption near the band edge can be calculated from the following Eq. (2) [39]:

$$\alpha h\nu = A(h\nu - E_g)^{n/2} \quad (2)$$

where α, h, ν, A and E_g are absorption coefficient, Planck constant, light frequency, a constant and band gap energy, respectively. Among them, n is determined by the type of optical transition of a semiconductor ($n=1$ for direct transition and $n=4$ for indirect transition). The value of n is 4 for BiOBr and 1 for TiO_2 [40]. The E_g can be thus estimated from a plot of $(\alpha h\nu)^{n/2}$ versus photon energy ($h\nu$). The intercept of the tangent to the X-axis will give a good approximation of the E_g for BiOBr and TiO_2. Plots of $(\alpha h\nu)^{n/2}$ versus photon energy ($h\nu$) of BiOBr and TiO_2 are shown in Fig. 5b. The estimated E_g of BiOBr and TiO_2 are about 2.6 and 3.2 eV, respectively. Since the $h_{Br\,4p}{}^{+}$ is 2.25 V, the conduction band edge potential of BiOBr is −0.35 V according to the formula $E_g = E_{vb} - E_{cb}$. Comparing with TiO_2, BiOBr exhibits a sharp increase absorption in the UV and visible light region, which allows photocatalytic degradation with BiOBr under a wide scope of wavelength and enhances the efficiency of photocatalytic behavior for organic contaminants.

3.2. Degradation pathways of CYN and uracil under UV and visible light illumination

HPLC-PDA was used to monitor the degradation process of CYN and uracil. As shown in Fig. 6, only 12.9% of CYN was adsorbed on the surface of BiOBr at adsorption equilibrium. Under UV light irradiation, 23.4% of CYN was photolyzed after 12 h. In contrast, 86.8% of CYN was degraded in the presence of BiOBr under otherwise identical conditions (Fig. 6a). Whereas, under visible light illumination, CYN was slightly photolyzed (<5%) without catalyst, and completely degraded in the presence of BiOBr after 3.5 h (Fig. 6b). As shown in Fig. 6c, the adsorption capacity of BiOBr toward uracil was low (<5%). Under UV light illumination, 21.2% of uracil was photolyzed without BiOBr, and 93.5% of uracil was degraded in the presence of BiOBr after 14 h. In contrast, only 6.9% of uracil was photolyzed in the absence of BiOBr, and completely degraded with BiOBr after 10 h of visible light irradiation (Fig. 6d). The intensity of visible light was higher than that of UV light, so the decomposition rates of CYN and uracil under visible light were faster than that under UV light. It was noted that the degradation rates of uracil are slower than the photodegradation of CYN under both UV and visible light, because the redox potential of uracil is lower than that of CYN.

The radical formation during the degradation was proved qualitatively by ESR, using the non-saturated anti-magnetic material DMPO as spin trapping agent to detect and identify short-lived free radicals (Fig. 7). In the traditional Fenton system, characteristic quartet peaks of DMPO-•OH adduct in aqueous solution with an intensity ratio of 1:2:2:1 appears rapidly, and the signal stabilizes after 92 s in dark (Fig. 7a). For the BiOBr photocatalytic systems, ESR results show that both •OH and $\bullet O_2^-$ generate under UV and visible light (Fig. 7b and c). However, •OH is the main radical because $\bullet O_2^-$ tends to transform into •OH [41].

The structures of the degradation products of CYN and uracil were obtained based on the analysis of total ion chromatograms (TIC) and the corresponding LC–MS results, which were summarized in Table 1. Most intermediates were abundant initially and gradually decrease with extending reaction time. Four intermediates were generated with strong peaks from the decomposition fragments of CYN by traditional Fenton reagents. The intermediates generated from the degradation of CYN by BiOBr under both UV and visible light were the same, but different from the products formed in Fenton system.

Table 1
Peak area (count × 10^5) of CYN degradation intermediates detected with LC–MS.

CYN/Fe^{2+}/H_2O_2							CYN/UV/BiOBr							CYN/Vis/BiOBr							Uracil/UV/BiOBr							Uracil/Vis/BiOBr						
RT (min)	9.1	5.6	7.1	7.6	10.9		RT (min)	9.1	5.6	10.1	11.1		RT (min)	9.1	5.7	10.0	10.3		RT (min)	9.2	3.5	3.5	3.6	3.7		RT (min)	9.2	3.5	3.5	3.6	3.7	
$[M+H]^+$ (m/z)	415.6	319.3	447.3	431.4	413.4		(m/z)	415.6	319.3	275.5	413.4		(m/z)	415.6	319.3	293.5	413.4		(m/z)	112.9	145.9	85.9	88.1	144.4		(m/z)	112.9	145.9	85.9	88.1	144.4	
t (min)							t (h)						t (h)						t (h)							t (h)						
0	5.32	0	0	0	0		0	5.18	0.75	0.82	0.03		0	5.31	0	0	0		0	1.23	0	0	0	0		0	0.82	0	0	0	0	
5	2.49	0.13	0.73	0.13	0.24		1	4.84	1.08	7.12	3.42		0.5	3.51	0.05	0.42	0.36		1	0.87	3.15	1.54	0.94	1.96		1	0.69	4.82	0.75	0.15	2.17	
10	1.02	0.24	1.54	0.14	0.29		2	4.16	1.26	6.85	3.79		1	2.17	0.07	0.58	0.38		2	1.04	3.45	2.14	0.97	2.48		2	0.52	4.93	0.60	0.13	3.05	
15	0.04	0.30	1.83	0.23	0.38		3	3.65	2.53	5.42	3.85		1.5	1.24	0.10	0.59	0.37		3	0.97	3.26	1.98	1.15	2.97		3	0.43	4.82	0.43	0.15	3.94	
30	0	0.14	0.15	0.09	0.03		4	2.68	1.83	4.93	3.98		2	0.82	0.09	0.69	0.36		4	0.87	3.07	2.06	1.67	2.86		4	0.35	4.65	0.56	0.15	3.84	
/	/	/	/	/	/		5	2.57	1.89	3.12	3.07		2.5	0.48	0.11	1.82	0.35		5	0.78	3.04	2.34	1.94	3.43		5	0.24	4.39	0.73	0.23	2.94	
/	/	/	/	/	/		6	2.11	1.51	2.95	2.71		3	0.18	0.12	2.98	0.28		6	0.68	2.26	2.31	2.57	3.71		6	0.13	4.51	0.54	0.19	2.71	
/	/	/	/	/	/		7	1.97	0.92	2.07	2.45		3.5	0.07	0.08	3.18	0.16		7	0.56	2.51	2.09	2.47	4.25		7	0.07	4.19	0.43	0.22	2.38	
/	/	/	/	/	/		8	1.83	0.37	1.83	2.02		/	/	/	/	/		8	0.55	1.98	1.95	2.59	4.02		8	0.005	2.89	0.63	0.18	1.03	
/	/	/	/	/	/		/	/	/	/	/		/	/	/	/	/		9	0.46	1.54	1.99	2.36	3.79		9	0	1.25	0.71	0.18	0.18	
/	/	/	/	/	/		/	/	/	/	/		/	/	/	/	/		10	0.36	0.94	0.92	2.21	3.22		/	/	/	/	/	/	
/	/	/	/	/	/		/	/	/	/	/		/	/	/	/	/		11	0.23	1.02	0.86	1.89	2.56		/	/	/	/	/	/	
/	/	/	/	/	/		/	/	/	/	/		/	/	/	/	/		12	0.19	0.74	0.77	1.17	1.96		/	/	/	/	/	/	

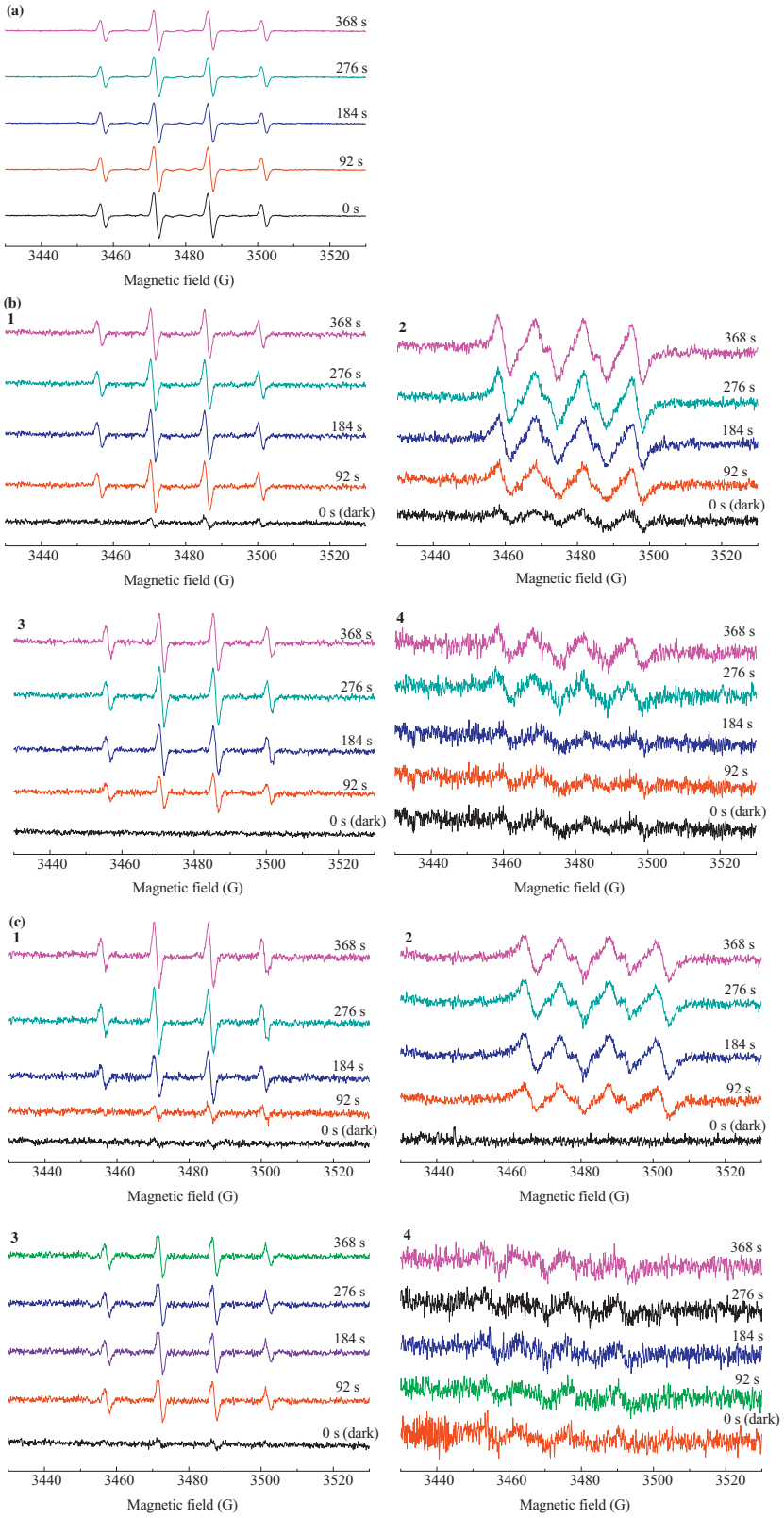

Fig. 7. ESR signals of the DMPO-•OH adducts in aqueous solution (panels 1 and 3) and DMPO-•O_2^- adducts in methanol (panels 2 and 4). Panels 1 and 2 were under UV light irradiation and panels 3 and 4 were under visible light irradiation in the systems of (a) Fe^{2+} and H_2O_2, (b) CYN and (c) uracil. [DMPO] = 0.04 mol/L, [Fe^{2+}] = 0.001 mol/L; [H_2O_2] = 0.025 mol/L; [BiOBr] = 5 g/L.

As shown in Fig. 8, the possible degradation pathways are proposed based on the degradation products. The addition of •OH at C15 of the C14–C15 double bond in the uracil ring forms a carbon radical. The stable product *m*/*z* 431 (1) generates from subsequent elimination of •H from C15. The product *m*/*z* 447 (2), originated from dihydroxylated product *m*/*z* 449, is from the addition of •OH to the C14–C15 double bond of electron-rich unsaturated uracil moiety in CYN. The oxidation of the secondary alcohol (bridging

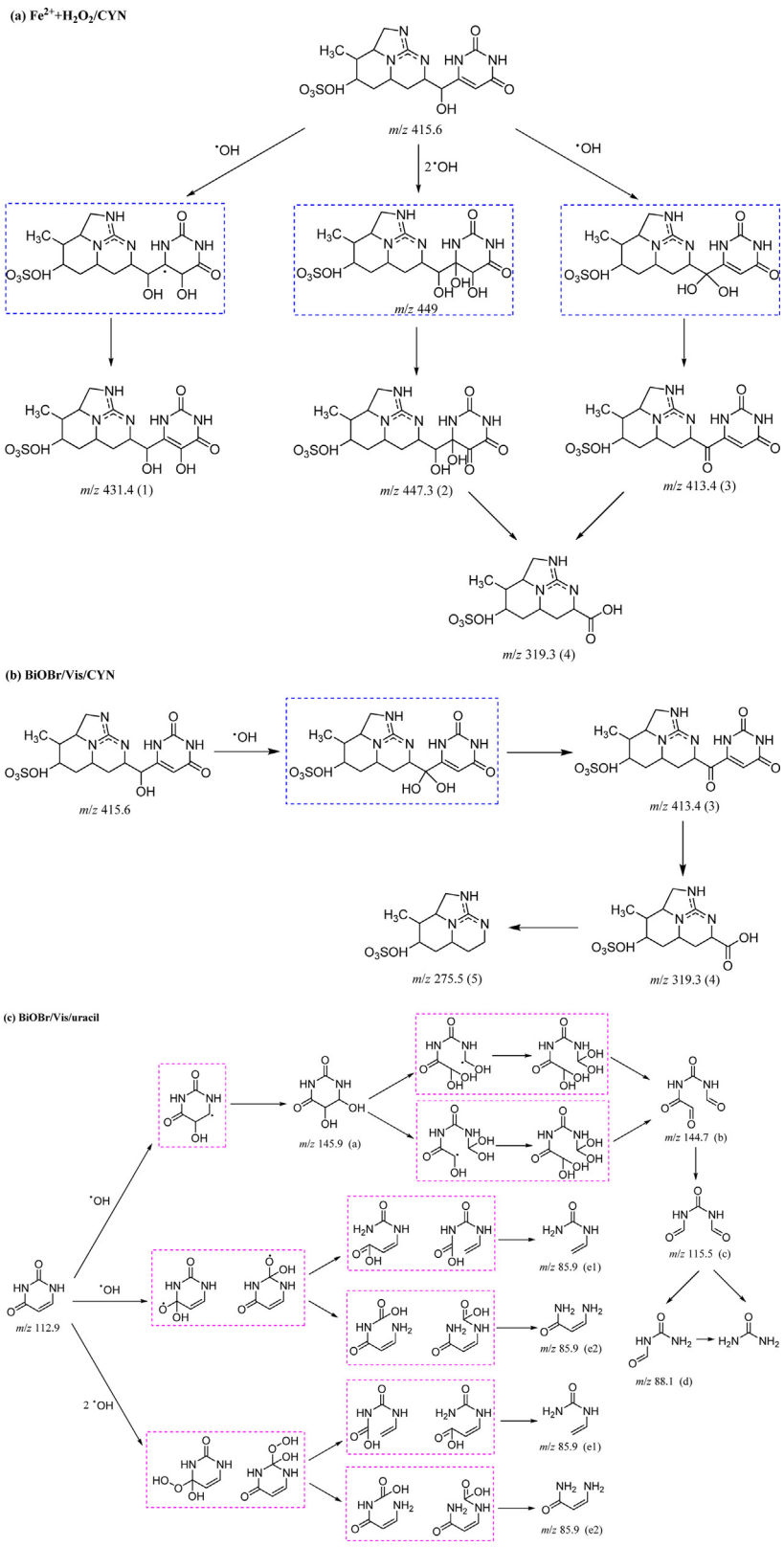

Fig. 8. Proposed pathways for the systems of (a) CYN degradation by Fenton reagents, (b) CYN degradation by BiOBr and (c) the degradation of uracil by BiOBr.

methine group) leads to the product *m*/*z* 413 (3) and the cleavage of uracil moiety easily occurs to generate the product *m*/*z* 319 (4). Therefore, the detoxification of CYN is through the cleavage of uracil moiety, which is the same as the oxidation by •OH generated from γ radiation [33]. For the degradation pathways of CYN by BiOBr photocatalysis systems, further investigation demonstrates that they are similar under UV and visible light irradiation (Fig. 8b). CYN is primarily transformed into the product *m*/*z* 413 (4) and then to *m*/*z* 319 (4). Compared with the products generated in the Fenton system, *m*/*z* 275 (5) identified at retention time of 10 min,

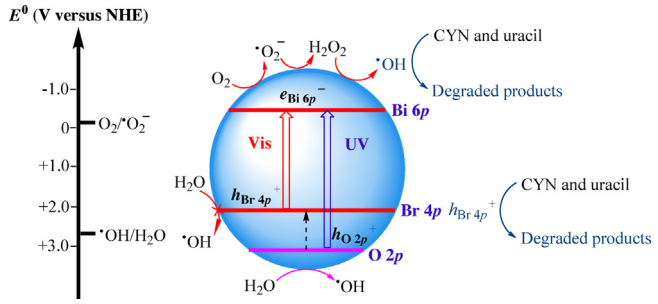

Fig. 9. Possible mechanisms of CYN and uracil photodegradation by BiOBr in aqueous solution.

corresponding to the loss of 44 mass unites from product *m*/*z* 319 (4), is assigned to the decarboxylation of it. Like the degradation of CYN, the intermediates from the degradation of uracil under UV and visible light are identified to propose a degradation pathway (Fig. 8c). Hydroxyl radical attacks the double bond of C5–C6 to yield the uracilglycol *m*/*z* 146 (a), which is then decomposed to aldehydic product *m*/*z* 144 (b). Further attack leads to a new dialdehyde product *m*/*z* 116 (c), which is finally converted to urea by means of an intermediate *m*/*z* 88 (d). Urea is possibly the final product. On the other hand, •OH attack easily occurs at C1 and C3 to generate the product *m*/*z* 86 (e).

The theoretical calculations were also performed. The results reveal that the electron population at C13 (3.98) and the bond order of C13–O28 (0.99) are low. So hydrogen abstraction reaction of the hydroxyl group at C13 occurs easily, which leads to the cleavage of uracil moiety. For uracil, the addition of •OH at the double bond C5–C6 is attributed to low free valence of C5 and C6 (0.49 and 0.44). Moreover, C1 and C3 are two easily attack sites for the electron population of them are 0.74 and 0.68, respectively. The bond orders of C1–N2, N2–C3 and C3–N4 are 0.43, 0.46 and 0.46, respectively, therefore the cleavage of them easily happens. The theoretical calculation results support the proposed degradation pathways very well.

3.3. Proposed mechanism

As shown in Fig. 9, a plausible mechanism for the degradation of CYN and uracil under UV and visible light is proposed. Our previous study revealed that BiOBr has two separate valence bands, O 2*p* and Br 4*p* states, which respond to UV and visible light for the potentials of $h_{O\,2p}^{+}$ and $h_{Br\,4p}^{+}$ were 3.1 V and 2.25 V, respectively. Although the two valence band holes generated have different oxidizing abilities and induce different reactions, the interband relaxation significantly reduces the difference between the UV and visible irradiation systems [32]. We can infer that the $h_{Br\,4p}^{+}$ formation from relaxation (UV system) or direct excitation (visible light system), initiates the oxidation of CYN and uracil. Consequently, the $h_{Br\,4p}^{+}$ induced oxidation of BiOBr photocatalytic systems under both UV and visible light irradiation is undoubtedly of the same kind.

Since the redox potential of $h_{Br\,4p}^{+}$ is not high enough to oxidize H_2O, the formation of high active species (•OH and $^{\bullet}O_2^{-}$) cannot from the oxidation of H_2O at valence band, but is attributed to the reduction of O_2 by conduction band electrons ($e_{Bi\,6p}^{-}$) on account of more negative potential of $e_{Bi\,6p}^{-}$ (−0.35 V) than that of $O_2/^{\bullet}O_2^{-}$ (−0.05 V). The substrates which can be oxidized increase the capture rate of $h_{Br\,4p}^{+}$, inhibit the recombination of $h_{Br\,4p}^{+}$ and $e_{Bi\,6p}^{-}$, and then facilitate the reduction of O_2 to •OH by $e_{Bi\,6p}^{-}$. In our experiment, CYN is more easily oxidized, so it is easy to be captured by $h_{Br\,4p}^{+}$, leading to more quick degradation rate.

In conclusion, both the degradation of CYN and uracil are attributed to the oxidation by $h_{Br\,4p}^{+}$ and $e_{Bi\,6p}^{-}$. The $h_{Br\,4p}^{+}$ has the ability to directly oxidize CYN and uracil. Meanwhile, the $e_{Bi\,6p}^{-}$ are easily transformed into high activity •OH which can degrade CYN and uracil.

4. Conclusions

The BiOBr promoted degradation of poisonous CYN under UV and visible light was studied. CYN was detoxified by removing the uracil moiety, which is the toxic unit of it. Under both UV and visible light, the degradation rate of uracil was lower than that of CYN. The formation of $h_{Br\,4p}^{+}$ from relaxation and direct excitation under UV and visible light, respectively, plays important roles in the oxidation of CYN and uracil. In spite of the $h_{Br\,4p}^{+}$ of BiOBr is not high enough to oxidize H_2O, •OH and $^{\bullet}O_2^{-}$ are generated at both UV and visible light systems for the reduction of O_2 by $e_{Bi\,6p}^{-}$. Consequently, the degradation of CYN and uracil are attributed to the oxidation by $h_{Br\,4p}^{+}$ and radical species (•OH and $^{\bullet}O_2^{-}$).

Acknowledgments

We thank Dr. David M. Johnson of Ferrum College (Ferrum, VA) for his assistance in revising the manuscript. This work was funded by the National Natural Science Foundation of China (Nos. 21377067, 21207079 and 21177072).

References

[1] I.R. Falconer, A.R. Humpage, Environ. Toxicol. 21 (2006) 299–304.
[2] P. Gallo, S. Fabbrocino, M.G. Cerulo, P. Ferranti, M. Bruno, L. Serpe, Rapid Commun. Mass Spectrom. 23 (2009) 3279–3284.
[3] P. Senogles, G. Shaw, M. Smith, R. Norris, R. Chiswell, J. Mueller, R. Sadler, G. Eaglesham, Toxicon 38 (2000) 1203–1213.
[4] H. Ken-ichi, O. Ikuko, I. Kayoko, S. Makoto, W.F. Mariyo, W. Masayuki, T. Kiyoshi, Toxicon 32 (1994) 73–84.
[5] A. Quesada, E. Moreno, D. Carrasco, T. Paniagua, L. Wormer, C. Hoyos, A. Sukenik, Eur. J. Phycol. 41 (2006) 39–45.
[6] A. Stüken, J. Rücker, T. Endrulat, K. Preussel, M. Hemm, B. Nixdorf, U. Karsten, C. Wiedner, Phycologia 45 (2006) 696–703.
[7] R.H. Li, W.W. Carmichael, S. Brittain, G.K. Eaglesham, G.R. Shaw, Y.D. Liu, M.M. Watanabe, J. Phycol. 37 (2001) 1121–1126.
[8] K. Preußel, A. Stüken, C. Wiedner, I. Chorus, J. Fastner, Toxicon 47 (2006) 156–162.
[9] L. Spoof, K.A. Berg, J. Rapala, K. Lahti, L. Lepistö, J.S. Metcalf, G.A. Codd, J. Meriluoto, Environ. Toxicol. 21 (2006) 552–560.
[10] M. Seifert, G. McGregor, G. Eaglesham, W. Wickramasinghe, G. Shaw, Harmful Algae 6 (2007) 73–80.
[11] A. Ballot, J. Fastner, C. Wiedner, Appl. Environ. Microbiol. 76 (2010) 1173–1180.
[12] D.J. Griffiths, M.L. Saker, Environ. Toxicol. 18 (2003) 78–93.
[13] R. Banker, S. Carmeli, M. Werman, B. Teltsch, R. Poratand, A. Sukenik, J. Toxicol. Environ. Health A 62 (2001) 281–288.
[14] L. Wormer, M. Huerta-Fontela, S. Cires, D. Carrasco, A. Quesada, Environ. Sci. Technol. 44 (2010) 3002–3007.
[15] S. Klitzke, S. Apelt, C. Weiler, J. Fastner, I. Chorus, Toxicon 55 (2010) 999–1007.
[16] S. Klitzke, C. Beusch, J. Fastner, Water Res. 45 (2011) 1338–1346.
[17] L. Ho, P. Lambling, H. Bustamante, P. Duker, G. Newcombe, Water Res. 45 (2011) 2954–2964.
[18] S. Merel, M. Clement, A. Mourot, V. Fessard, O. Thomas, Sci. Total Environ. 408 (2010) 3433–3442.
[19] S. Merel, M. Clement, O. Thomas, Toxicon 55 (2010) 677–691.
[20] E. Rodríguez, G.D. Onstad, T.P.J. Kull, J.S. Metcalf, J.L. Acero, U.V. Gunten, Water Res. 41 (2007) 3381–3393.
[21] E. Rodríguez, A. Sordo, J.S. Metcalf, J.L. Acero, Water Res. 41 (2007) 2048–2056.
[22] G.D. Onstad, S. Strauch, J. Meriluoto, G.A. Codd, U.V. Gunten, Environ. Sci. Technol. 41 (2007) 4397–4404.
[23] M. Mohajerani, M. Mehrvar, F. Ein-Mozaffari, Int. J. Eng. 3 (2009) 120–146.
[24] M. Pelaez, P. Falaras, A.G. Kontos, A.A. Cruz, K. Oshea, P.S.M. Dunlop, J.A. Byrne, D.D. Dionysiou, Appl. Catal. B: Environ. 121–122 (2012) 30–39.
[25] P.J. Senogles, J.A. Scott, G. Shaw, H. Stratton, Water Res. 35 (2001) 1245–1255.
[26] J. Xu, W. Meng, Y. Zhang, L. Li, C.S. Guo, Appl. Catal. B: Environ. 107 (2011) 355–362.
[27] M. Shang, W.Z. Wang, L. Zhang, J. Hazard. Mater. 167 (2009) 803–809.
[28] M.A. Gondal, X.F. Chang, M.A. Ali, Z.H. Yamani, Q. Zhou, G.B. Ji, Appl. Catal. A: Gen. 397 (2011) 192–200.
[29] W.L. Huang, Q.S. Zhu, J. Comput. Chem. 30 (2008) 183–190.
[30] Y.F. Fang, Y.P. Huang, J. Yang, P. Wang, G.W. Cheng, Environ. Sci. Technol. 45 (2011) 1593–1600.
[31] X. Zhang, Z.H. Ai, F.L. Jia, L.Z. Zhang, J. Phys. Chem. C 112 (2008) 747–753.

[32] Y.F. Fang, W.H. Ma, Y.P. Huang, G.W. Cheng, Chem. Eur. J. 19 (2013) 3224–3229.
[33] W.H. Song, S.W. Yan, W.J. Cooper, D.D. Dionysiou, K.E. OShea, Environ. Sci. Technol. 46 (2012) 12608–12615.
[34] U. Norinder, J. Mol. Struct. 151 (1987) 259–269.
[35] S. Yasuko, S. Yoshiya, JACS 100 (1978) 67–72.
[36] E. Estrada, M. Benzi, Chem. Phys. Lett. 568–569 (2013) 184–189.
[37] M. Galceran, M.C. Pujol, C. Zaldo, F. Díaz, M. Aguiló, J. Phys. Chem. C 113 (2009) 15497–15506.
[38] Y.N. Huo, J. Zhang, M. Miao, Y. Jin, Appl. Catal. B: Environ. 111–112 (2012) 334–341.
[39] M.A. Butler, J. Appl. Phys. 48 (1977) 1914–1920.
[40] K.L. Zhang, C.M. Liu, F.Q. Huang, C. Zheng, W.D. Wang, Appl. Catal. B: Environ. 68 (2006) 125–129.
[41] M.R. Hoffmann, S.T. Martin, W.Y. Choi, D.W. Bahnemann, Chem. Rev. 95 (1995) 69–96.